Appl Phys B (2012) 107:483–487
DOI 10.1007/s00340-012-4956-2

Applied Physics B
Lasers and Optics

Broadband downconversion based near-infrared quantum cutting via cooperative energy transfer in $YNbO_4:Bi^{3+}$, Yb^{3+} phosphor

R. Zhou · Y. Kou · X. Wei · C. Duan · Y. Chen · M. Yin

Received: 13 July 2011 / Published online: 21 March 2012

Abstract $YNbO_4:Bi^{3+}$, Yb^{3+} phosphor was prepared to study the quantum cutting process of converting one ultraviolet photon into two near-infrared photons. An intense near-infrared emission of Yb^{3+}:$^2F_{5/2} \rightarrow {}^2F_{7/2}$ around 1 μm was observed under the ultraviolet excitation belonging to the broadband absorption of the $[NbO_4]^{3-}$ group and the Bi^{3+} ion. The photoluminescence spectra and decay lifetime measurements indicate efficient energy transfer from Bi^{3+} to Yb^{3+} ions, which is attributed to be of a cooperative energy transfer mechanism. The $YNbO_4:Bi^{3+}$, Yb^{3+} phosphor with optimized doping concentration may be applicable in improving the efficiency of silicon-based solar cells.

Keywords Photoluminescence · Near-infrared quantum cutting · Cooperative energy transfer

1 Introduction

One of the major challenges in photovoltaic research today is to increase solar cell conversion efficiency by making better use of the solar spectrum [1, 2]. Considerable research recently has been focused on better exploitation of the solar cells via a photon conversion process in order to use this environmentally friendly energy source for future energy demands [3–7]. The most popular solar cells are based on crystalline Si (c-Si) and the band gap of c-Si is about 1.12 eV (∼1100 nm). The process of quantum cutting (QC) can convert one photon of high energy into two photons of lower energy [8]. If conversion of one incident ultraviolet (UV) or visible photon into two near-infrared (NIR) photons is realized, the main energy loss in solar cells due to the thermalization of charge carriers generated by the absorption of high-energy photons will be minimized. Fortunately, rare-earth (RE) ions with abundant energy levels are good candidates for the QC process. The research on QC systems started from single ions capable of cascade emission such as Pr^{3+} [9, 10], Tm^{3+} [11], and Gd^{3+} [12]. Then, the combination of two ions like the Gd^{3+}–Eu^{3+} couple [8] through stepwise energy transfer aroused extensive attention of researchers. A QC process based on cooperative energy transfer (CET) was reported in $Yb_xTb_{1-x}PO_4:Tb^{3+}$ powder by Vergeer et al. [13] in 2005. Via CET, two NIR photons at 980 nm from the emission of Yb^{3+}can be obtained by the excitation of one Tb^{3+} ion with one blue photon. Since then, a similar NIR QC phenomenon has been extensively reported in RE codoped systems such as Tb^{3+}–Yb^{3+} [14, 15], Tm^{3+}–Yb^{3+} [16], and Pr^{3+}–Yb^{3+} [17]. The single emission around 1000 nm of the Yb^{3+} ion matches well with the band gap of c-Si, so it is a good choice to realize the conversion of incident UV or visible photons into NIR photons via the QC process. However, the NIR emission of Yb^{3+} in the RE^{3+}/Yb^{3+} systems mentioned above is very weak due to the inefficient excitation of the donors for their parity-forbidden 4f–4f transitions. Though the Ce^{3+}–Yb^{3+} [18] system overcomes this shortcoming, the combination of Ce^{3+}–Yb^{3+} codopant is unstable [19, 20]. Recently, strong Yb^{3+} NIR emission has been reported utilizing the efficient energy transfer from the host YVO_4 to Yb^{3+} [21]. However, the relatively low quenching concentration and the toxicity of the raw material may restrict its practical application in Si-based solar cells. Another phosphor studied to achieve efficient NIR QC via CET is $Gd_2O_3:Bi^{3+}$, Yb^{3+} [22], where the Bi^{3+} ion was chosen as an activator. The absorption band

R. Zhou · Y. Kou · X. Wei · C. Duan · Y. Chen · M. Yin (✉)
Department of Physics, University of Science and Technology of China, Hefei 230026, China
e-mail: yinmin@ustc.edu.cn
Fax: +86-551-3607417

in Gd_2O_3:Bi^{3+}, Yb^{3+} due to the transition between localized electronic energy levels of $Bi^{3+}$is neither intense nor broad enough. Thus, other QC materials are still urgently needed to be developed to enhance the energy conversion efficiency via spectral modification.

The host material, $YNbO_4$, is a well-known self-activated phosphor, all the niobate groups of which may be considered as fluorescent centers [23]. The self-luminescent complex $[NbO_4]^{3-}$ in $YNbO_4$ shows a broad and strong emission band in the spectral region around 400 nm while the absorption band ranges from about 200 to 300 nm. The luminescent property is ascribed to the ligand–metal charge transfer (CT) transition of tetrahedral $[NbO_4]^{3-}$ molecular ions [24, 25]. The emission wavelength and intensity can be modified by introducing dopant ions into the host. The RE ions can easily replace the Y^{3+} ions for the similar properties between Y^{3+} and other RE ions. So, it is expected that the doping concentration of the RE ions can be high. The photoluminescence properties of $YNbO_4$ activated by RE ions such as Eu^{3+}, Dy^{3+}, Sm^{3+}, and Er^{3+} [26, 27] have been reported.

Bi^{3+} is a typical type of localized activator with strong electric-dipole-allowed $s^2 \rightarrow sp$ transition. The main emission band is $^3P_1 \rightarrow {}^1S_0$ which is nominally spin forbidden but has nevertheless reasonably high oscillator strength [28]. When a phosphor is doped with Bi^{3+} ions as activators, the position of the main excitation band varies depending on the nature of the host lattice. RE niobates are efficient hosts for Bi^{3+} known as self-activated luminescent materials. Introducing Bi^{3+} into $YNbO_4$ shifts the emission band to the longer wavelength of 440 nm [29], making $YNbO_4$:Bi^{3+} a suitable and efficient blue phosphor for field emission display (FED) application [30]. Compared with the undoped $YNbO_4$, the blue photon emitted from $YNbO_4$:Bi^{3+} matches much better the energies of two Yb^{3+}: $^2F_{7/2} \rightarrow {}^2F_{5/2}$ transitions, making the CET from one Bi^{3+} to two Yb^{3+} theoretically possible and potentially more efficient. Besides, the doping of the Bi^{3+} ion extends the absorption band due to the superposition of the charge transfer of $[NbO_4]^{3-}$ and the Bi^{3+}: $6s^2 \rightarrow 6s6p$ electric-dipole-allowed transition [31, 32]. The broader absorption band in the UV part leads to better utilization of the solar spectrum. The present work demonstrates the NIR QC phenomenon in $YNbO_4$:Bi^{3+}, Yb^{3+} phosphors via the CET process.

2 Experimental

Powder samples of $Y_{0.99-x}Yb_xBi_{0.01}NbO_4$ ($x = 0$, 2 %, 8 %, 16 %, 32 %, and 48 %) were prepared by a conventional solid-state reaction method using Y_2O_3 (99.99 %), Nb_2O_5 (99.5 %), Bi_2O_3 (99.9 %), and Yb_2O_3 (99.99 %) as starting materials. A stoichiometric mixture of the raw materials was ground and calcined in an alumina crucible at

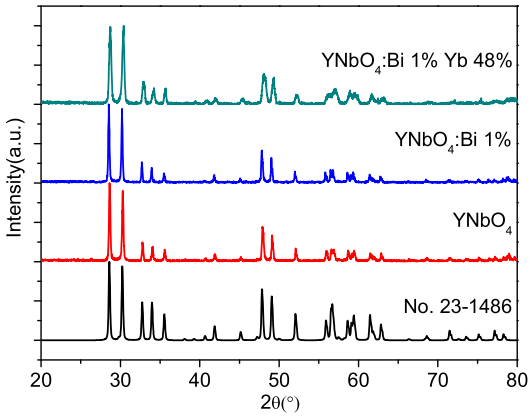

Fig. 1 XRD patterns of $YNbO_4$, $Y_{0.99}Bi_{0.01}NbO_5$, and $Y_{0.51}Yb_{0.48}Bi_{0.01}NbO_5$ samples as synthesized. *Bottom*: standard profiles of $YNbO_4$ (JCPDS 23-1486)

1200 °C for 4 h in air. The crystalline phases of the synthesized samples were identified via an X-ray diffractometer (XRD, MAC Science Co. Ltd., MXPAHF) using Cu Kα radiation in the range of $2\theta = 20$–80°; the accelerating voltage was 30.0 kV and the tube current was 160.0 mA. The excitation and emission spectra were obtained with a Jobin–Yvon Fluorolog 3 system. For the lifetime measurements, a Q-switched frequency-quadrupled (266 nm) Nd:YAG laser with a pulse duration of 10 ns was used and the signal was analyzed with a Tektronix TDS2024 digital storage oscilloscope. The visible emission was dispersed by a Jobin-Yvon HRD1 double monochromator and was detected by a Hamamatsu R928 photomultiplier. The NIR emission was dispersed by a Zolix SBP750 monochromator and was detected by an Acton ID-441-C InGaAs NIR detector. The signal was analyzed by an EG&G7265 DSP lock-in amplifier and stored into computer memories. The spectra were recorded under identical experimental conditions so that the emission intensities of the samples with different Yb^{3+} doping concentrations can be compared. All the measurements were carried out at room temperature.

3 Results and discussion

Figure 1 shows the representative XRD patterns of $YNbO_4$, $Y_{0.99}Bi_{0.01}NbO_4$, and $Y_{0.51}Yb_{0.48}Bi_{0.01}NbO_4$ samples as synthesized. It can be seen that all the diffraction peaks for the samples can be well assigned to the reported data of monoclinic $YNbO_4$ (JCPDS 23-1486). No obvious shifting of peaks or second phase can be detected at the current doping level, indicating that the introduction of Bi^{3+} and Yb^{3+} ions does not change the crystal structure of the powder. This may be due to their similar ionic radii (Y^{3+}, $r = 0.089$ nm; Bi^{3+}, $r = 0.096$ nm; Yb^{3+}, $r = 0.086$ nm).

The concentration of Bi^{3+} is fixed at the optimal doping level of 1 mol %. The photoluminescence excitation

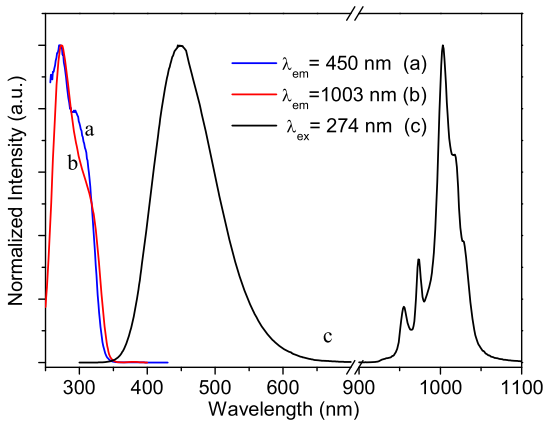

Fig. 2 PLE and PL spectra of $YNbO_4$: Bi 1 mol %, Yb 16 mol %: (**a**) monitored at 450 nm, (**b**) monitored at 1003 nm, and (**c**) excited at 274 nm

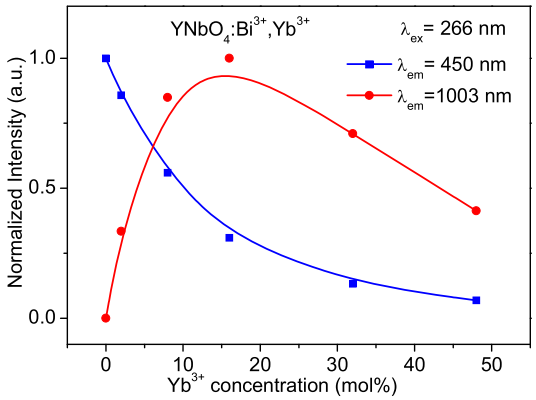

Fig. 3 The dependence of Bi^{3+} (450 nm) and Yb^{3+} (1003 nm) emission intensities on the Yb^{3+} concentration in $YNbO_4$:Bi^{3+}, Yb^{3+}

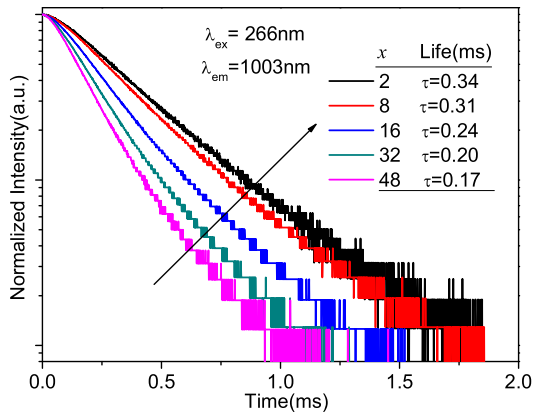

Fig. 4 The decay curves of the Yb^{3+}: $^2F_{5/2} \rightarrow {}^2F_{7/2}$ luminescence at 1003 nm for the samples $YNbO_4$:Bi^{3+} 1 mol %, Yb^{3+} x mol % ($x = 2$, 8, 16, 32, and 48) upon 266-nm excitation

(PLE) and photoluminescence (PL) spectra of $YNbO_4$:Bi^{3+} 1 mol %, Yb^{3+} 16 mol % are presented in Fig. 2. A broad excitation band ranging from 250 to 350 nm was recorded when 450 nm was monitored (Fig. 2a). The peak centered at about 274 nm is most likely assigned to an electron transition of the molecular orbital of $[NbO_4]^{3-}$ while the shoulder around 294 nm is obviously a Bi effect that influences the optical properties of the $[NbO_4]^{3-}$ group. Electronic structure calculations of $YNbO_4$ indicated that the conduction band is composed of Nb 4d orbitals and the valence band of O 2p orbitals [29]. The Bi 6s6p is located at a lower energy level than that of Nb 4d. The calculated partial densities of states show that the Bi $6s^2$ valence band levels lie just above the O 2p valence band levels and the Bi $6s^2$ levels overlap with the O 2p ones [29, 32]. Thus, the electron in O 2p (Bi $6s^2$) can be excited to Nb 4d and Bi 6s6p. The broad absorption band is attributed to the combined action of the $[NbO_4]^{3-}$ group and the Bi ion. By monitoring the Yb^{3+}: $^2F_{5/2} \rightarrow {}^2F_{7/2}$ transition at 1003 nm (Fig. 2b), a similar broad excitation band was also recorded. The essential coincidence of the two excitation spectra reveals the identical energy origin of the visible emission and NIR emission. Under the excitation of 274 nm (Fig. 2c), a broad blue emission centered at 450 nm was observed. According to Ref. [31], when Bi^{3+} is introduced into $YNbO_4$, the excited Nb 4d electron is transferred to Bi 6s6p. Then, the 6s6p $\rightarrow$ $6s^2$ transition produces the 450-nm emission. Since the Bi 6s6p levels overlap with the O 2p ones, it is expected that the emission is due to transitions inside the Bi electronic energy levels and transitions between Bi and O via CT [33]. Besides the blue emission from Bi^{3+} ions, there is an intense emission band peaking at 1003 nm along with several small shoulders. Since the Bi^{3+} ions do not contribute to NIR emission [34], this NIR emission is attributed to the $^2F_{5/2} \rightarrow {}^2F_{7/2}$ Stark level transitions of Yb^{3+} ions.

The dependence of Bi^{3+} and Yb^{3+} emission intensities on various Yb^{3+} concentrations in $YNbO_4$:Bi^{3+}, Yb^{3+} phosphors is shown in Fig. 3. Emission intensities were recorded under 266-nm excitation with identical conditions at room temperature for all the samples. It is noticed that the intensity of Bi^{3+} emission decreases monotonically with the increase of the Yb^{3+} concentration, whereas the intensity of Yb^{3+} emission first reaches a maximum at a concentration of 16 mol % and then gradually decreases with further increase of concentration. This is a common phenomenon called concentration quenching. Many factors lead to the concentration quenching of Yb^{3+} ions which plays a negative effect on the Yb^{3+} NIR emission, including an increased amount of impurities and an increased possibility of energy migration to the quenching centers [15, 21]. The decay curves of Yb^{3+} emission at 1003 nm upon excitation of 266 nm are shown in Fig. 4. The lifetime decreases monotonically from 0.34 to 0.17 ms with Yb^{3+} concentration increasing from 2 to 48 mol %, verifying the Yb^{3+} concentration quenching process that results from increased migra-

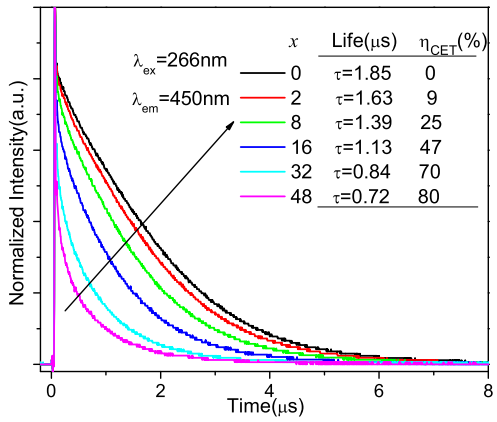

Fig. 5 The decay curves of the Bi^{3+} emission at 450 nm for the samples $YNbO_4$:Bi^{3+} 1 mol %, Yb^{3+} x mol % ($x = 2$, 8, 16, 32, and 48) upon 266-nm excitation. The inset shows the calculated CET efficiency (η_{CET}) as a function of x

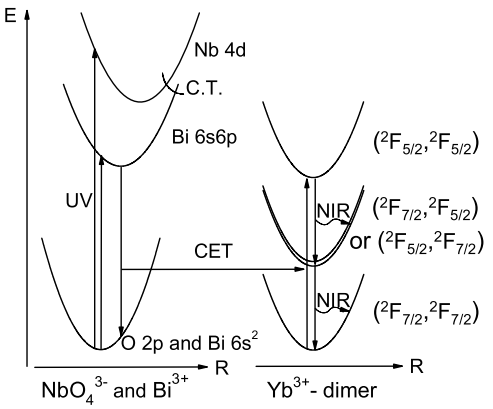

Fig. 6 Schematic configuration coordinate diagram for $[NbO_4]^{3-}$, Bi^{3+}, and Yb^{3+}, and the CET process for the NIR QC emission

tion. The variation of emission intensities of Bi^{3+} and Yb^{3+} emission intensities on Yb^{3+} doping concentration is further indicative of energy transfer from Bi^{3+} to Yb^{3+}.

In Fig. 5, the decay curves for Bi^{3+} emission at 450 nm are plotted for various Yb^{3+} concentrations. An obvious trend is that the lifetime of the Bi^{3+} emission decreases with increasing Yb^{3+} concentration. The lifetime is about 1.85 μs for the sample without Yb^{3+} while it is reduced to 0.72 μs when the Yb^{3+} concentration is 48 mol %. Since the only variable for different samples is the Yb^{3+} concentration, the fast decline of the lifetime is naturally ascribed to the incorporation of Yb^{3+} ions. Yb^{3+} doping provides an extra decay pathway: energy transfer from Bi^{3+} to Yb^{3+} that accelerates the Bi^{3+} emission decay rate. The result is considered to be a further proof of the efficient energy transfer from Bi^{3+} to Yb^{3+}. The non-exponential decay is a character of the decay of donors, which have a fluctuating distribution of surrounding acceptors Yb^{3+}.

Generally, the O^{2-}–Yb^{3+} CT band is located at the relatively high energy region with wavelength shorter than 250 nm [35]. It has also been pointed out that the CT absorption band is higher in energy for Yb^{3+} than for Eu^{3+} in the same host lattice, and the CT absorption band of Eu^{3+} is located in about the range of 230–260 nm [36, 37]. Hence, there is no influence of O^{2-}–Yb^{3+} CT on Bi^{3+} and Yb^{3+} emissions, and the intense UV-excited NIR emissions can only be attributed to the energy transfer from $[NbO_4]^{3-}$ and Bi^{3+} to Yb^{3+}, since the Yb^{3+} ion has no levels in the UV region. Due to the absence of the energy overlap between the emission of the Bi^{3+} ion and a single Yb^{3+} ion and the existence of the resonance between the emission energy of Bi^{3+} and twice the photon energy of absorption of Yb^{3+}, we conclude that the $Bi^{3+} \rightarrow Yb^{3+}$ CET process is the only possible energy transfer process to achieve the Yb^{3+} NIR emission. The variation of emission intensities of Bi^{3+} and Yb^{3+} on Yb^{3+} doping concentration and the increased decay rates for Bi^{3+} emission with increasing Yb^{3+} concentration support this.

Figure 6 pictures the schematic configuration coordinate diagram for $[NbO_4]^{3-}$, Bi^{3+}, and Yb^{3+} as well as the CET process for the NIR QC emission. Since the Bi 6s6p levels overlap with the O 2p ones, at the excitation of a UV photon, an electron situated in the O 2p (Bi $6s^2$) valence band is excited to the excited energy levels consisting of Nb 4d orbitals of $[NbO_4]^{3-}$ groups and the lower Bi 6s6p levels. The excitation will reside in the lowest 6s6p levels before relaxing by emission or via CET to two Yb^{3+} ions, which subsequently emit two NIR photons.

From the luminescence decay curves shown in Fig. 5, the CET efficiency (η_{CET}) and the total theoretical downconversion quantum efficiency (η_{QE}) could be calculated by the following equations [13]:

$$\eta_{CET} = 1 - \frac{\int I_{x\ \%\ Yb}\,dt}{\int I_{0\ \%\ Yb}\,dt}, \tag{1}$$

$$\eta_{QE} = \eta_{Bi}(1 - \eta_{CET}) + 2\eta_{Yb}\eta_{CET}, \tag{2}$$

where I denotes the decay intensity, x % Yb stands for the Yb^{3+} concentration, and η_{Bi} and η_{Yb} refer to the internal quantum efficiencies of Bi^{3+} and Yb^{3+}, respectively. With Yb^{3+} concentration increasing from 0 to 48 mol %, the CET efficiency from Bi^{3+} to Yb^{3+} increases monotonically from 0 to 80 % as shown in the inset of Fig. 5. Supposing that the excited Yb^{3+} decay radiatively ($\eta_{Yb} = 1$) for the sample $YNbO_4$:Bi^{3+} 1 mol %, Yb^{3+} 2 mol % with the lifetime $\tau_{2\ \%\ Yb} = 0.34$ ms, the quantum efficiencies of Yb^{3+} (η_{Yb}) could be estimated from the lifetimes of Yb^{3+} emission by the following equation:

$$\eta_{Yb} = \frac{A_R}{A_{total}}, \tag{3}$$

where $A_{total} = 1/\tau_{x\ \%\ Yb}$, representing the total decay rate for the samples with various Yb^{3+} doping concentrations,

and $A_R = A_{total} = 1/\tau_{2\ \%\ Yb}$ is considered as concentration independent. The calculated η_{Yb} is 1, 0.91, 0.71, 0.59, and 0.50 for the samples with Yb^{3+} doping concentrations of 2, 8, 16, 32, and 48 mol %, respectively. The decrease of Yb^{3+} internal quantum efficiency is due to concentration quenching. Meanwhile, assuming that all the excited Bi^{3+} decay radiatively ($\eta_{Bi} = 1$), for the samples with the Yb^{3+} doping concentrations of 2, 8, 16, 32, and 48 mol %, the total quantum efficiency is calculated to be 109 %, 121 %, 120 %, 113 %, and 100 %. However, if the value of η_{Yb} is promoted to approach 1 by reducing the concentration of quenching centers, an upper limit of the theoretical quantum efficiency of 109 %, 125 %, 147 %, 170 %, and 180 % will be reached for these samples with the Yb^{3+} doping concentrations of 2, 8, 16, 32, and 48 mol %, respectively. A maximum quantum efficiency of 180 % is close to the limit of 200 % for the case of ideal one-to-two QC.

4 Conclusion

Efficient broadband NIR QC $YNbO_4$:Bi^{3+}, Yb^{3+} phosphor that converts UV photons which are almost useless in the silicon solar cell to NIR photons around 1 μm where the Si solar cell exhibits the most efficient spectral response has been successfully developed. A CET mechanism was proposed to rationalize the process. The PLE and PL spectra and decay lifetime measurements evidence the occurrence of CET from Bi^{3+} to Yb^{3+} ions with quantum efficiencies higher than 100 %. The NIR QC $YNbO_4$:Bi^{3+}, Yb^{3+} phosphor with reduced concentration quenching and optimized doping concentration may reach 180 % in quantum efficiency and serve as a spectral modifier to enhance the photovoltaic conversion efficiency of silicon-based solar cells.

Acknowledgements This work was financially supported by the National Natural Science Foundation of China (Grant Nos. 10904139, 11011120083, 11111120060, and 11074245), the Knowledge Innovation Project of the Chinese Academy of Sciences (Grant No. KJCX2-YW-M11), the China Postdoctoral Science Foundation (Grant No. 20100480693), and the Special Foundation for Talents of Anhui Province, China (Grant No. 2007Z021).

References

1. A. Luque, A. Martí, A. Bett, V.M. Andreev, C. Jaussaud, J.A.M. Van Roosmalen, J. Alonso, A. Räuber, G. Strobl, W. Stolz, C. Algora, B. Bitnar, A. Gombert, C. Stanley, P. Wahnon, J.C. Conesa, W.G.J.H.M. van Sark, A. Meijerink, G.P.M. van Klink, K. Barnham, R. Danz, T. Meyer, I. Luque-Heredia, R. Kenny, C. Christofides, G. Sala, P. Benítez, Sol. Energy Mater. Sol. Cells **87**, 467 (2005)
2. A. Shalav, B.S. Richards, T. Trupke, K.W. Krämer, H.U. Güdel, Appl. Phys. Lett. **86**, 013505 (2005)
3. W.G.J.H.M. van Sark, Appl. Phys. Lett. **87**, 151117 (2005)
4. E. Klampaftis, D. Ross, K.R. McIntosh, B.S. Richards, Sol. Energy Mater. Sol. Cells **93**, 1182 (2009)
5. A. Shalav, B.S. Richards, T. Trupke, K.W. Krämer, H.U. Güdel, Appl. Phys. Lett. **86**, 013505 (2005)
6. M. Peng, L. Wondraczek, J. Mater. Chem. **19**, 627 (2009)
7. H. Shpaisman, O. Niitsoo, I. Lubomirsky, D. Cahen, Sol. Energy Mater. Sol. Cells **92**, 1541 (2008)
8. R.T. Wegh, H. Donker, K.D. Oskam, A. Meijerink, Science **283**, 663 (1999)
9. W.W. Piper, J.A. DeLuca, F.S. Ham, J. Lumin. **8**, 344 (1974)
10. J.L. Sommerdijk, A. Bril, A.W. de Jager, J. Lumin. **8**, 341 (1974)
11. R. Pappalardo, J. Lumin. **14**, 159 (1976)
12. R.T. Wegh, H. Donker, A. Meijerink, R.J. Lamminmäki, J. Hölsä, Phys. Rev. B **56**, 13841 (1997)
13. P. Vergeer, T.J.H. Vlugt, M.H.F. Kox, M.I. den Hertog, J.P.J.M. van der Eerden, A. Meijerink, Phys. Rev. B **71**, 014119 (2005)
14. Q.Y. Zhang, C.H. Yang, Z.H. Jiang, X.H. Ji, Appl. Phys. Lett. **90**, 061914 (2007)
15. X. Liu, S. Ye, Y. Qiao, G. Dong, B. Zhu, D. Chen, G. Lakshminarayana, J. Qiu, Appl. Phys. B **96**, 51 (2009)
16. L.C. Xie, Y.H. Wang, H.J. Zhang, Appl. Phys. Lett. **94**, 061905 (2009)
17. B.M. van der Ende, L. Aarts, A. Meijerink, Adv. Mater. **21**, 3073 (2009)
18. D. Chen, Y. Wang, Y. Yu, P. Huang, F. Weng, J. Appl. Phys. **104**, 116105 (2008)
19. G. Blasse, B.C. Grabmaier, *Luminescent Materials* (Springer, Berlin, 1994)
20. J.W.M. Verweij, C. Pedrini, D. Bouttet, C. Dujardin, H. Lautesse, B. Moine, Opt. Mater. **4**, 575 (1995)
21. X.T. Wei, S. Huang, Y.H. Chen, C.X. Guo, M. Yin, W. Xu, J. Appl. Phys. **107**, 103107 (2010)
22. X.Y. Huang, Q.Y. Zhang, J. Appl. Phys. **107**, 063505 (2010)
23. G. Blasse, Philips Res. Rep. **23**, 344 (1968)
24. D.A. Grisafe, C.W. Fritsch, J. Solid State Chem. **17**, 313 (1976)
25. G. Blasse, K.C. Bleijenberg, R.C. Powell, *Luminescence and Energy Transfer* (Springer, Heidelberg, 1980)
26. A.M.G. Massabni, G.J.M. Montandon, M.A. Couto dos Santos, Mater. Res. **1**, 1 (1998)
27. B. Yan, X. Xiao, J. Alloys Compd. **433**, 251 (2007)
28. J.L. Sommerdijk, J.M.P.J. Verstegen, A. Bril, Philips Res. Rep. **29**, 517 (1974)
29. C. Han, H. Kim, H. Chang, S.K. Lee, H.D. Park, J. Electrochem. Soc. **147**, 2800 (2000)
30. A. Vecht, D. Charlesworth, D.W. Smith, in *Dig. Tech. Papers SID Int. Symp.*, Boston (1997), p. 588
31. S.H. Shin, D.Y. Jeon, K.S. Suh, J. Appl. Phys. **90**, 5986 (2001)
32. S.K. Lee, H. Chang, C.H. Han, H.J. Kim, H.G. Jang, H.D. Park, J. Solid State Chem. **156**, 267 (2001)
33. J.H. Bahng, E.S. Oh, S.H. Seo, J.S. Kim, M. Lee, H.L. Park, C. Lee, G.C. Kim, K.J. Kim, Phys. Status Solidi A **191**, 291 (2002)
34. M. Peng, L. Wondraczek, J. Mater. Chem. **19**, 627 (2009)
35. P. Dorenbos, J. Phys., Condens. Matter **15**, 8417 (2003)
36. L. van Pieterson, M. Heeroma, E. de Heer, A. Meijerink, J. Lumin. **91**, 177 (2000)
37. X. Xiao, B. Yan, Appl. Phys. A **88**, 333 (2007)